Supplementary information: Dynamics and Resilience of the Unconventional Charge Density Wave in ScV_6Sn_6 Bilayer Kagome Metal

Manuel Tuniz[1†], Armando Consiglio[2†], Denny Puntel[1], Chiara Bigi[3], Stefan Enzner[2], Ganesh Pokharel[4], Pasquale Orgiani[5], Wibke Bronsch[6], Fulvio Parmigiani[1,6], Vincent Polewczyk[5], Phil D. C. King[3], Justin W. Wells[7], Ilija Zeljkovic[8], Pietro Carrara[5,9], Giorgio Rossi[5,9], Jun Fujii[5], Ivana Vobornik[5], Stephen D. Wilson[4], Ronny Thomale[2], Tim Wehling[10,11], Giorgio Sangiovanni[2], Giancarlo Panaccione[5], Federico Cilento[6*], Domenico Di Sante[12, 13*], Federico Mazzola[5, 14*]

[1]Dipartimento di Fisica, Università degli studi di Trieste, Trieste, 34127, Italy.

[2]Institut für Theoretische Physik und Astrophysik and Würzburg-Dresden Cluster of Excellence ct.qmat, Universität Würzburg, Würzburg, 97074,Germany.

[3]School of Physics and Astronomy, University of St Andrews,St Andrews, KY16 9SS, United Kingdom.

[4]Materials Department, University of California Santa Barbara, Santa Barbara, 93106, California, USA.

[5]Istituto Officina dei Materiali, Consiglio Nazionale delle Ricerche,Trieste, I-34149, Italy.

[6]Elettra - Sincrotrone Trieste S.C.p.A.,Trieste, Strada Statale 14, km 163.5, Italy.

[7]Centre for Materials Science and Nanotechnology, University of Oslo (UiO), Oslo, 0318, Norway.

[8]Department of Physics, Boston College, Chestnut Hill, MA, 02467, USA.

[9]Dipartimento di Fisica, Università degli Studi di Milano, Milano, via Celoria 16, 20133, Italy.

[10]Institute of Theoretical Physics, University of Hamburg, Hamburg, Notkestrasse 9, 22607, Germany.

[11]The Hamburg Centre for Ultrafast Imaging, Hamburg, Luruper Chaussee 149, 22761, Germany.
[12]Department of Physics and Astronomy, University of Bologna, Bologna, 40127, Italy.
[13]Center for Computational Quantum Physics, Flatiron Institute, Bologna, 162 5th Avenue, New York, NY 10010, USA.
[14]Department of Molecular Sciences and Nanosystems, Ca' Foscari University of Venice, Venice, 30172, Italy.

*Corresponding author(s). E-mail(s): federico.cilento@elettra.eu; domenico.disante@unibo.it; federico.mazzola@unive.it;
†These authors contributed equally to this work.

Supplementary Note 1. High-resolution Fermi Surfaces and ARPES measurements along the $\bar{\Gamma}$-$\bar{K}$ direction across the critical temperature

Here, we show additional ARPES measurements collected with various light polarization and both above and below the transition temperature. Both Fermi surfaces and energy versus momentum maps are shown (See Supplementary Fig. 1).

Supplementary Note 2. ARPES and measurements without surface states

The ARPES measurements have been performed across the transition temperature, i.e. 98 K, for ScV_6Sn_6 both with and without the present of surface states. While the surface states presence is guaranteed by a successful UHV cleave, in order to suppress them and to remain on the same sample's spot precautions are needed. Indeed, we noticed that by cleaving the samples both at 16 K and at 120 K (in the CDW phase and above it) the surfaces states are present. However, if one cleaves the samples at 16 K (or at 120 K) and varies the temperature up to 120 K (or down to 16 K) the surface states are killed, possibly to absorption onto the sample's following a temperature change. To a suppression of the surface states an overall reduction of the ARPES data quality was observed. In order to get high quality surface states, as in the main text, we cleaved the same sample one time at 16 K and one time at 120 K. Then, in order to detect the bulk electronic structure as in S1, we waited a sufficient time at the selected temperature until the surface states were suppressed by aging. This ensures a better overall quality of the ARPES data, compared to a forced aging by thermal process, and allows us to be sure to be on the same area of the sample with the light beam. We noticed also a variation in the aging time. For samples cleaved at 120 K,

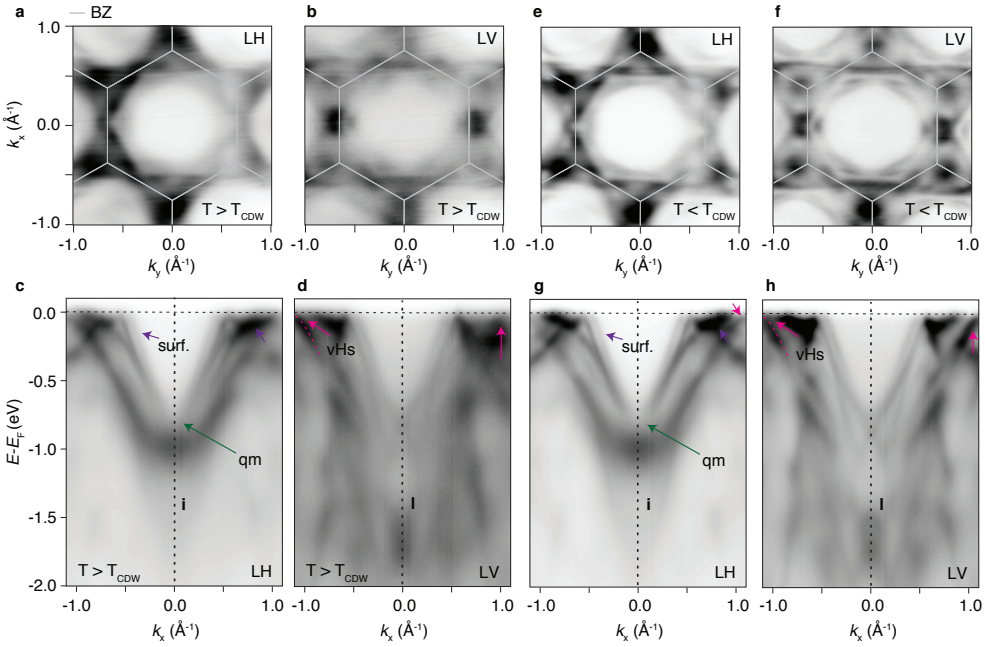

Supplementary Fig. 1 Measured electronic structure of ScV_6Sn_6 across the CDW critical temperature. Fermi surface of ScV_6Sn_6 collected above T_{CDW} by using linear **a** horizontal and **b** vertical light polarizations and **c-d** corresponding energy versus momentum dispersion along the $\bar{\Gamma}$-$\bar{K}$-$\bar{M}$ direction of the Brillouin zone. Fermi surface of ScV_6Sn_6 collected below T_{CDW} by using linear **e** horizontal and **f** vertical light polarizations and **g-h** corresponding energy versus momentum dispersion along the $\bar{\Gamma}$-$\bar{K}$-$\bar{M}$ direction of the Brillouin zone. In the figure, 'surf' indicates a surface state contribution, 'qm' the quadratic minimum of parabolic bands [1].

despite the initial lower quality, the surface states resisted for a longer time, i.e. 15-24 hours. For samples cleaved at 16 K, we noticed an initial better quality for the ARPES data, but a faster degradation time of about 4-6 hours. For the data in the main text, above the transition temperature, the surface states appear weaker. Such a weaker intensity recorded for the surface states above T_{CDW} is not surprising given the more pronounced degradation expected for the highest temperature cleave. In this regard, we even noticed that by increasing slightly further the temperature, the surface states get completely suppressed. However, the electronic structure remains the same, with no changes in van-Hove singularities (red arrows in Fig.2 of the main text) and overall dispersion.

Supplementary Note 3. Identification of the surface states and their quality

ScV_6Sn_6, similarly to other kagome metals, is characterized by the presence of surface states, after the ultrahigh vacuum (UHV) cleave. These surface states have been

extensively discussed for other kagome systems [2–4], other members of the 166 family [1, 5–9], and also recently reported for ScV_6Sn_6 itself [10]. By comparing our results with those of Ref.[10], we found a surface termination clearly consistent with the spectral weight of a V_3Sn area: the surface states at the K-points (not observed for the $ScSn_2$ termination), the vanishing intensity of the parabolic states close to the quadratic minimum (see 'qm' in Supplementary Fig. 1 **c** and **g**), and the absence of the small pocket at $\bar{\Gamma}$ and at the Fermi level observed for the Sn_2 termination, are evidence of this attribution [10]. It is crucial to point out that the type of surface termination obtained after the cleave is irrelevant to our study, having the CDW a marked bulk character.

Supplementary Note 4. Tr-OS analysis and details

In order to describe the incoherent part of the $\Delta R/R$ signal, we used a double-exponential function, $\Delta R/R \propto A_1 e^{-t/\tau_1} + A_2 e^{-t/\tau_2} + bkg$, where $A_1 e^{-t/\tau_1}$ describes the fast decay process (first stage of the CDW) while $A_2 e^{-t/\tau_2}$ describes the slower recovery process (second stage of the CDW). The bkg term is used to take into account an extremely slow recovery process that can be described by a constant value in our time window.

In order to quantitatively analyze the oscillatory component of the $\Delta R/R$ signal, we considered the Fourier transform of the residuals obtained by considering the difference between the data and the double-exponential fit function described above. The complete fit function, resulting in the black lines of Fig.3 of the main text, has been obtained by adding a damped cosine oscillation, $A_p e^{-t/\tau_p} cos(w_p t + \phi_p)$.

To give a rough estimate the induced heating by the pump, we assumed, reasonably, that the heat capacity of ScV_6Sn_6 is of the same order of magnitude of the ones reported for similar kagome systems (both binary and ternary). We do not expect that the temperature deviates more than 20 K upon pump application.

Supplementary Note 5. Electronic and phononic band structures details

In this section are reported complementary figures, supporting the statements and the results of the main text. In particular, we report the calculated electronic structure with and without CDW separately (Supplementary Fig. 8), and the phonon density of states and the mechanism by which the phonon frequency has been estimated (Supplementary Fig. 9). In addition (Supplementary Fig. 10), we also show the data from time-resolved optical spectroscopy documenting the evolution of the fast component. Such evolution is reminiscent of the one observed in time-resolved photoelectron spectroscopy, and associated to the electronic degrees of freedom.

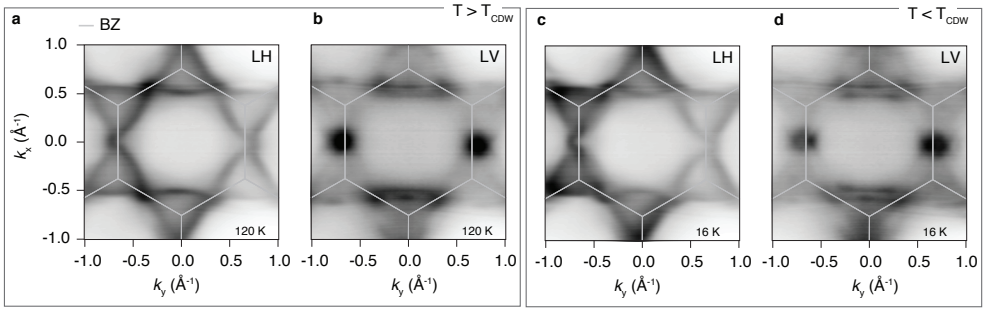

Supplementary Fig. 2 Fermi surfaces of ScV_6Sn_6 kagome metal without surface states. **a** Linear horizontal and **b** linear vertical polarization Fermi surface maps collected for ScV_6Sn_6 above the transition temperature. **c** Linear horizontal and **d** linear vertical polarization Fermi surface maps collected for ScV_6Sn_6 below the transition temperature. In order to be sure about the absence of surface states, the samples were left for a significant time in the same positions and same conditions (approximately 24 h) and they showed a natural aging effect, which resulted in the removal of the surface states manifold.

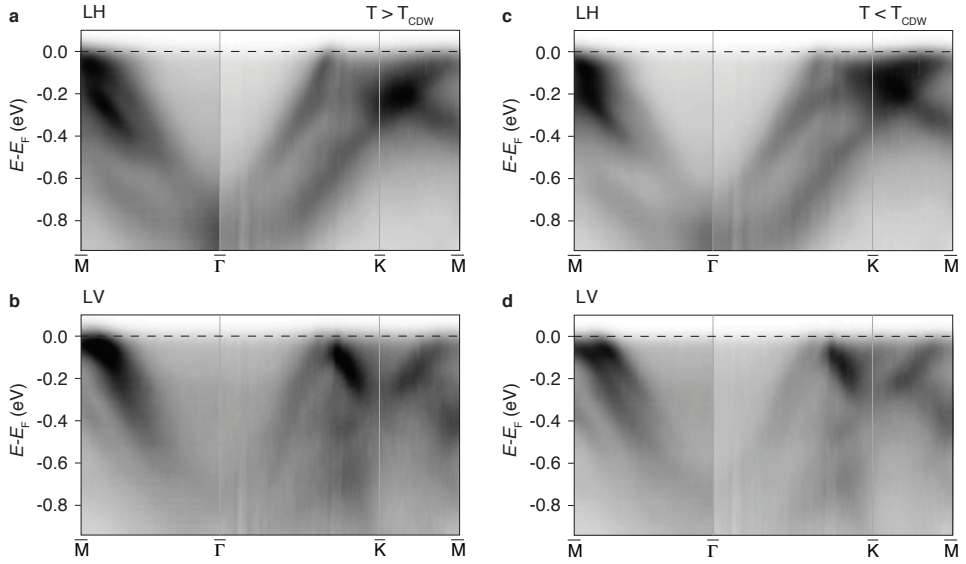

Supplementary Fig. 3 Energy vs momentum dispersion of ScV_6Sn_6 kagome metal without surface states. **a** linear horizontal and **b** vertical polarization spectra along the $\bar{\Gamma}$-$\bar{K}$-$\bar{M}$ direction of the BZ obtained for ScV_6Sn_6 after the surface states were suppressed as in S1, above T_{CDW}. **c** linear horizontal and **d** vertical polarization spectra along the $\bar{\Gamma}$-$\bar{K}$-$\bar{M}$ direction of the BZ obtained for ScV_6Sn_6 after the surface states were suppressed as in S1, below T_{CDW}.

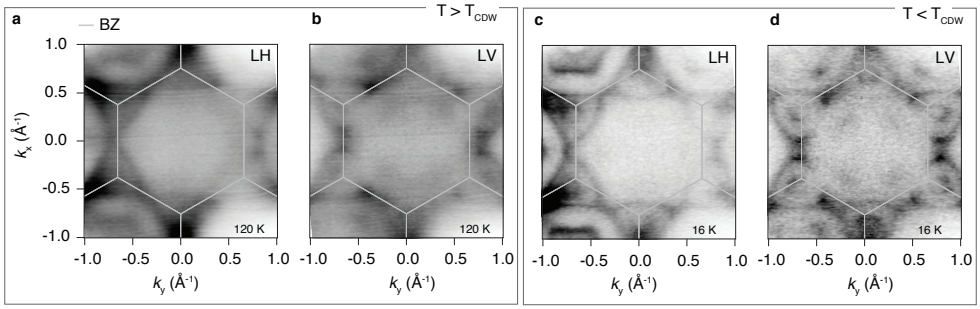

Supplementary Fig. 4 Fermi surfaces of ScV_6Sn_6 kagome metal, additional data. a Linear horizontal and **b** linear vertical polarization Fermi surface maps collected for ScV_6Sn_6 above the transition temperature. **c** Linear horizontal and **d** linear vertical polarization Fermi surface maps collected for ScV_6Sn_6 below the transition temperature. As one can see, the low temperature data appear sharper due to the reduced thermal broadening.

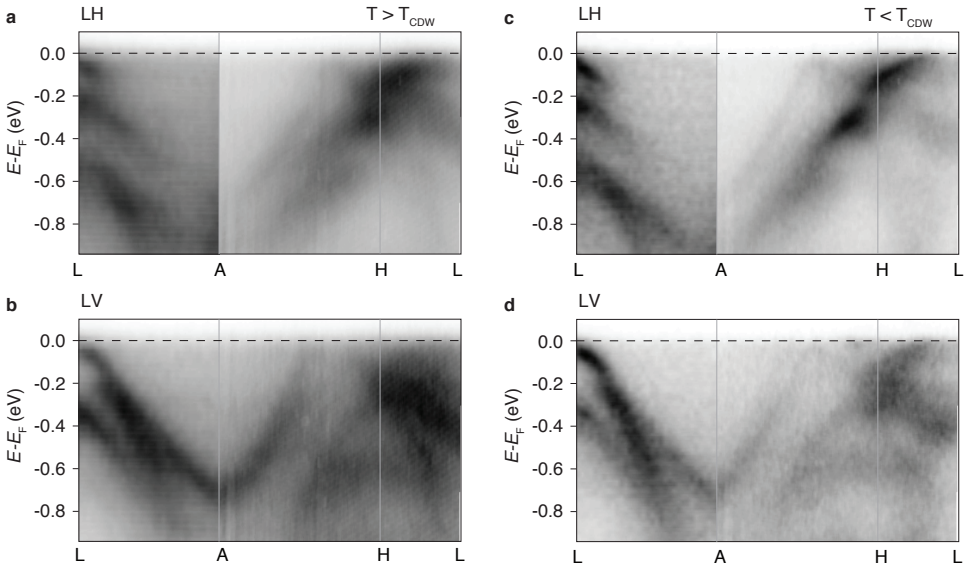

Supplementary Fig. 5 Energy vs momentum dispersion of ScV_6Sn_6, additional data set. a linear horizontal and **b** vertical polarization spectra at 65 eV for ScV_6Sn_6, above T_{CDW}. **c** linear horizontal and **d** vertical polarization spectra collected within the same conditions, below T_{CDW}. The data have been taken in a direction which we identified as *L-A-H-L*. This was done from the knowledge of the c-axis parameter, 0.923 nm and by assuming an inner potential of 12 eV (different inner potential values do not give rise to large variations in the k_z positioning).

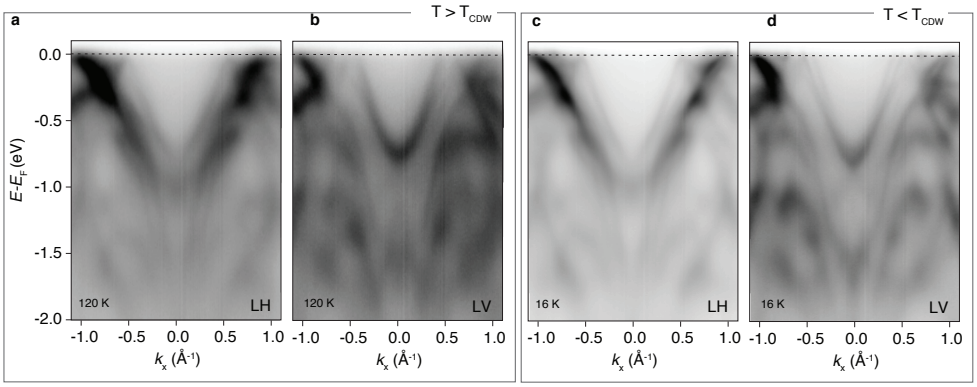

Supplementary Fig. 6 High-resolution Energy vs momentum dispersion of ScV_6Sn_6 kagome metal along a direction parallel to the A-H-L directions. a linear horizontal and **b** vertical polarization spectra at 65 eV obtained for ScV_6Sn_6, above T_{CDW}. **c** linear horizontal and **d** vertical polarization spectra with the same conditions, below T_{CDW}.

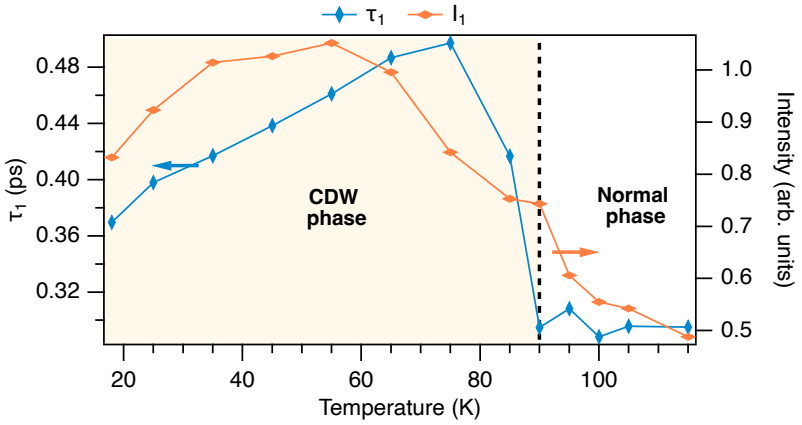

Supplementary Fig. 7 Fast decay evolution as function of temperature. Evolution of the lifetime (τ_1, left axis) and of the amplitude (I_1, right axis) of the first fast decay as a function of the temperature. As one can see, contrary to the amplitude decay as function of fluence (Fig. 4 of the main taxt), which shows a saturation, here, I_1 has a very similar behaviour to the lifetime as function of temperature.

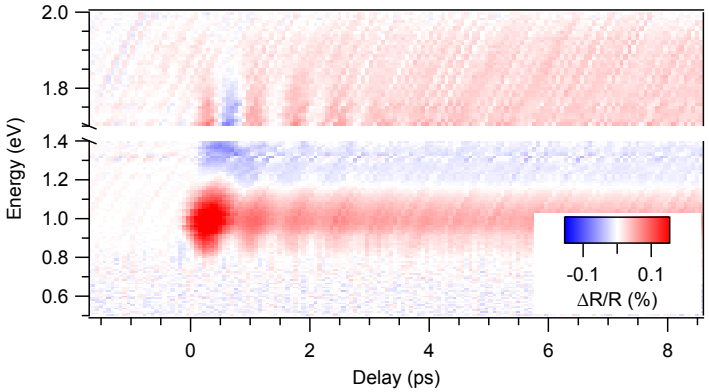

Supplementary Fig. 8 Time- and frequency- resolved reflectivity. The reflectivity is reported as energy versus time for samples kept at 30 K.

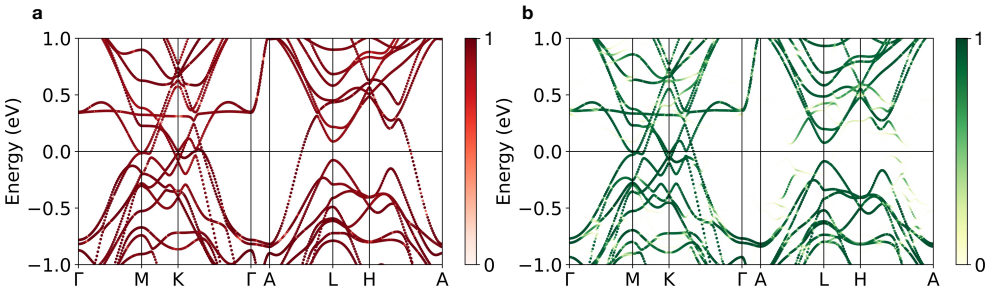

Supplementary Fig. 9 Band structure unfolding of the pristine phase vs the CDW one. **a** Electronic band structure of the pristine phase, with color-bar on the right side. The plot has been obtained unfolding the same superlattice of the CDW phase, without the lattice distortion. The bands have been shifted upward by 0.029 eV. **b** Electronic band structure of the CDW phase, with color-bar on the right side. Note how, in this case, a wider range of colors needs to be employed.

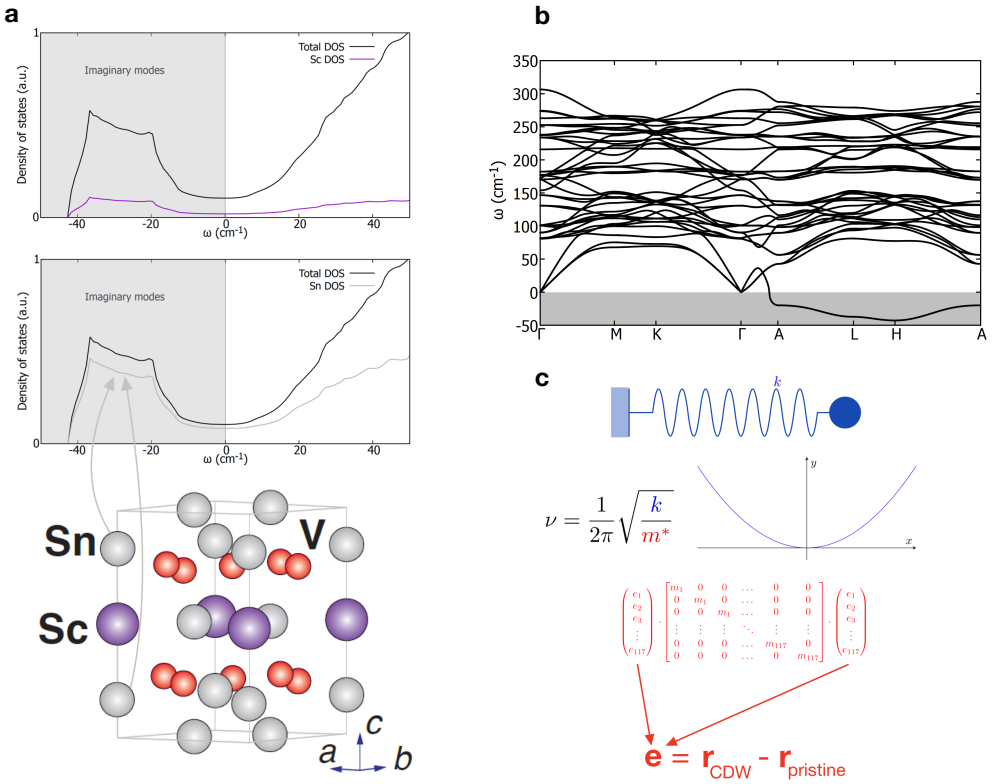

Supplementary Fig. 10 Phonon and CDW theoretical details. a Density of states of phonons in ScV_6Sn_6. The imaginary modes, indicating a dynamical instability, are only due to the Sc atom, and the two Sn atoms with the same scandium's (x, y) coordinates, from which the grey arrows start. **b** Phonons' dispersion in ScV_6Sn_6. **c** Schematic sketch of the procedure followed to compute the frequency of the phonon mode ($\nu = 1.42$ THz). Red colors refer to the effective mass m^*, obtained from the mass tensor and the (normalized) displacement vector. Blue color refers to the spring constant, obtained by doubling the quadratic coefficient of the parabola. This parabola has been obtained via a quadratic fit, about one of the two minima of the double-well potential energy profile.

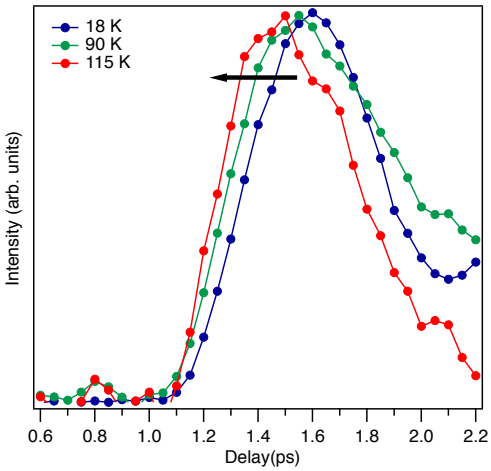

Supplementary Fig. 11 Evolution of the rising edge as function of time and temperature. Evolution of the rising edge of the ΔR/R signal at the arrival of the pump pulse, for three selected temperatures (below T_{CDW}, at T_{CDW} and above T_{CDW}). Above the critical temperature the maximum of the $\Delta R/R$ signal is reached 150 fs faster than in the CDW phase. The three traces have been normalized at their maximum intensity.

Supplementary References

[1] Di Sante, D., Bigi, C., Eck, P., Enzner, S., Consiglio, A., Pokharel, G., Carrara, P., Orgiani, P., Polewczyk, V., Fujii, J., King, P.D.C., Vobornik, I., Rossi, G., Zeljkovic, I., Wilson, S.D., Thomale, R., Sangiovanni, G., Panaccione, G., Mazzola, F.: Flat band separation and robust spin berry curvature in bilayer kagome metals. Nature Physics **19**, 1135–1142 (2023) https://doi.org/10.1038/s41567-023-02053-z

[2] Kang, M., Fang, S., Kim, J.-K., Ortiz, B.R., Ryu, S.H., Kim, J., Yoo, J., Sangiovanni, G., Di Sante, D., Park, B.-G., Jozwiak, C., Bostwick, A., Rotenberg, E., Kaxiras, E., Wilson, S.D., Park, J.-H., Comin, R.: Twofold van Hove singularity and origin of charge order in topological kagome superconductor CsV_3Sb_5. Nature Physics **18**(3), 301–308 (2022)

[3] Kang, M., Fang, S., Ye, L., Po, H.C., Denlinger, J., Jozwiak, C., Bostwick, A., Rotenberg, E., Kaxiras, E., Checkelsky, J.G., Comin, R.: Topological flat bands in frustrated kagome lattice CoSn. Nature Communications **11**(1), 4004 (2020) https://doi.org/10.1038/s41467-020-17465-1

[4] Kang, M., Ye, L., Fang, S., You, J.-S., Levitan, A., Han, M., Facio, J.I., Jozwiak, C., Bostwick, A., Rotenberg, E., Chan, M.K., McDonald, R.D., Graf, D., Kaznatcheev, K., Vescovo, E., Bell, D.C., Kaxiras, E., Brink, J., Richter, M., Prasad Ghimire, M., Checkelsky, J.G., Comin, R.: Dirac fermions and flat bands in the ideal kagome metal FeSn. Nature Materials **19**(2), 163–169 (2020) https://doi.org/10.1038/s41563-019-0531-0

[5] Pokharel, G., Teicher, S.M.L., Ortiz, B.R., Sarte, P.M., Wu, G., Peng, S., He, J., Seshadri, R., Wilson, S.D.: Electronic properties of the topological kagome metals YV_6Sn_6 and GdV_6Sn_6. Phys. Rev. B **104**, 235139 (2021) https://doi.org/10.1103/PhysRevB.104.235139

[6] Peng, S., Han, Y., Pokharel, G., Shen, J., Li, Z., Hashimoto, M., Lu, D., Ortiz, B.R., Luo, Y., Li, H., Guo, M., Wang, B., Cui, S., Sun, Z., Qiao, Z., Wilson, S.D., He, J.: Realizing kagome band structure in two-dimensional kagome surface states of RV_6Sn_6(R= Gd, Ho). Phys. Rev. Lett. **127**, 266401 (2021) https://doi.org/10.1103/PhysRevLett.127.266401

[7] Ishikawa, H., Yajima, T., Kawamura, M., Mitamura, H., Kindo, K.: GdV_6Sn_6: A Multi-carrier Metal with Non-magnetic 3d-electron Kagome Bands and 4f-electron Magnetism. Journal of the Physical Society of Japan **90**(12), 124704 (2021) https://doi.org/10.7566/JPSJ.90.124704

[8] Rosenberg, E., DeStefano, J.M., Guo, Y., Oh, J.S., Hashimoto, M., Lu, D., Birgeneau, R.J., Lee, Y., Ke, L., Yi, M., Chu, J.-H.: Uniaxial ferromagnetism in the kagome metal TbV_6Sn_6. Phys. Rev. B **106**, 115139 (2022) https://doi.org/10.1103/PhysRevB.106.115139

[9] Hu, Y., Wu, X., Yang, Y., Gao, S., Plumb, N.C., Schnyder, A.P., Xie, W., Ma, J., Shi, M.: Tunable topological Dirac surface states and van Hove singularities in kagome metal GdV_6Sn_6. Science Advances **8**(38), 2024 (2022)

[10] Lee, S., Won, C., Kim, J., Yoo, J., Park, S., Denlinger, J., Jozwiak, C., Bostwick, A., Rotenberg, E., Comin, R., et al.: Nature of charge density wave in kagome metal ScV_6Sn_6. arXiv preprint arXiv:2304.11820 (2023)